

Original Research

Effects of Soil Moisture on Surface Radiation Balance and Water-Heat Flux in Desert Steppe Environment of Inner Mongolia

Chang Yaowen^{1,2}, Zhang Lixing¹, Ding Jing¹, Wu Xueqin¹, Liu Xiaoxi¹, Xie Yunhu³, Gao Wenbang⁴, Hai Chunxing¹, Zhang Ruiqiang^{2*}

¹College of Geographical Science, Inner Mongolia Normal University, Hohhot 010022, Inner Mongolia, China

²The Institute of Water Resources for Pastoral Areas, Hohhot 010020, Inner Mongolia, China

³College of Desert Control Science and Engineering, Inner Mongolia Agricultural University, Hohhot 010018, China

⁴Faculty of Geographical Science, Beijing Normal University, Beijing 100875, China

Received: 15 March 2020

Accepted: 30 August 2020

Abstract

The response of surface radiation and water-heat flux to soil moisture is a critical mechanism in drought, desertification and other effects of climate change. This study analyzed soil moisture data and four-component radiation data during the summers (June, July and August) from 2010 to 2018 in a desert steppe environment of Inner Mongolia. The influence of soil moisture on the radiation flux and water-heat flux under dry, intermediate and wet conditions were quantified through correlation analysis. Radiation and water-heat fluxes showed obvious diurnal changes under different soil moisture conditions. Net longwave radiation and soil heat flux showed the largest differences in diurnal variation followed by net surface radiation, total flux and albedo. Net radiation, net longwave radiation, surface received longwave radiation, soil heat flux and total flux all increased with increasing soil moisture, while surface reflection ability decreased. Soil moisture during wet intervals (16.57-28%) showed a stronger correlation with fluxes than dry and intermediate intervals (9.78-16.46%). This indicates that soil moisture exerts a stronger influence on surface flux under moist conditions. Soil moisture showed a negative correlation with surface reflecting longwave radiation ($P<0.01$) and a positive correlation with net longwave radiation, net surface radiation and total flux ($P<0.01$). The research shows that soil moisture interacts with the atmospheric system through its influence on total flux (sensible heat and latent heat) and surface net radiation.

Keywords: desert steppe, soil moisture, surface albedo, net surface radiation, soil heat flux

Introduction

As the interface between the land and the atmosphere, soils play an important climatic role on different spatio-temporal scales. Numerous, complex interactions between the air and land [1,2] depend on both the land type and atmospheric condition [3]. Soil moisture is a key land parameter in this coupled system that can induce various climate feedback loops [4]. Vegetation cover and topography [5] can also influence soil moisture thereby increasing the complexity of interactions between the land surface and the atmosphere.

Surface soil represents a major reservoir of water. Soil moisture arises from the combined inputs of precipitation, evaporation and infiltration [6]. Previous studies [7-9] have shown that soil moisture plays a major role in atmospheric changes. On land, soil moisture exerts a greater influence on precipitation than sea surface temperature (SST). Studies estimate that 65% of global atmospheric precipitation comes from evaporation from the land surface [10]. Other studies have shown that changes in soil moisture influence summer atmospheric circulation in North America but this influence varies significantly in different regions [8]. The influence of changes in soil moisture on atmospheric precipitation and temperature also varies with time. Soil moisture for example appears to exert a greater influence on precipitation and temperature during summer, when atmospheric convection is stronger [11, 12]. Mass exchange and energy transmission between the land and atmosphere determine the influence of soil moisture on temperature and precipitation [13]. Studies [14-17] have found that soil moisture induces atmospheric effects mainly through surface albedo, near-surface soil heat flux and sensible / latent heat flux between land and air. As a result, different regions have different land-air coupling due to unique surface properties. The influence of soil moisture on temperature is mainly achieved by controlling the distribution of net radiation [18]. In Asia, there is a strong land-air coupling in the wet and dry climate transition regions in summer, including Northeast China, Eastern China, Northwest China, Mongolia, Southern Siberia, and Northern India [19]. Additional research addressing the correlation between early soil moisture and precipitation showed that the strong land-air coupling zone occurred primarily in the arid and semi-arid transition zone [20]. Determining the role of soil moisture in the surface energy radiation balance can therefore help elucidate land-air coupling mechanisms in these unique environments. Although some studies have explored the effects of soil moisture on surface radiation and water-heat fluxes, these have focused on the Tibetan plateau [21-23] and the eastern monsoon region [17, 24]. Few studies have addressed arid and semi-arid regions in northwest China.

The desert steppe region of Inner Mongolia is a typical transition zone between humid monsoon and

inland arid regions [25]. Precipitation occurs primarily during the summer, atmospheric convection is strong, and seasonal variation is significant. This region is also sensitive to climate change. In 2002, the Institute of Water Resources for Pastoral Areas of China established a comprehensive experimental base in this area to conduct long-term monitoring of land surface processes. This study addresses surface radiation through water-heat flux and meteorological data from the experimental base. The objectives were to: (1) clarify the daily character of radiation flux and water-heat flux under different wet and dry soil conditions, (2) determine the influence of soil moisture on net surface radiation, surface albedo, each radiant flux and soil heat flux and (3) explore feedback mechanisms within the coupled land-air system influenced by soil moisture. Generally, this research provides a theoretical basis for understanding land-air interactions in a desert steppe region.

Material and Methods

Study Area

The study area includes the area around Xilamuren Town (111°12'E, 41°21'N), a community located in the southeast of Darhan Muminggan United Banner, Baotou, Inner Mongolia (Fig. 1). The local terrain consists of low, gently sloping hills with an average altitude of 1600 m. The study area experiences a temperate continental monsoon climate characterized by dry and windy spring and autumn seasons, concentrated rainfall in summer and cold, dry winters. Mean annual precipitation is 282 mm and a mean annual air temperature in 4.2°C. Approximately 70-80% of the annual precipitation occurs from July to August. The study area experiences an annual wetness of 0.13-0.31, annual accumulated temperature of 1985-2800°C, 3100-3300 h of average annual sunshine, 83 d frost-free and an average annual evaporation capacity of 2503 mm. This exceeds annual precipitation by a factor of nine. The average wind speed is 4.5 m/s, and the maximum wind speed is 27.0 m/s with most wind from a north and northwest direction. The soil type is chestnut soil, and the soil texture is sandy loam soil. Vegetation consists of *Stipa krylovii* Roshev, the founding flora, and dominant species *Artemisia frigida*, *Cleistogenes squarrosa*, *Convolvulus ammannii* Desr, *Heteropappus altaicus*, *Agropyron cristatum* and *Leymus chinensis*.

Data and Processing

Data analyzed by this study were collected with an ENVIS automatic weather station (IMKO Company, Germany) and a UGT water erosion observation system (UGT company, Germany) installed within a meteorological observation unit maintained by the

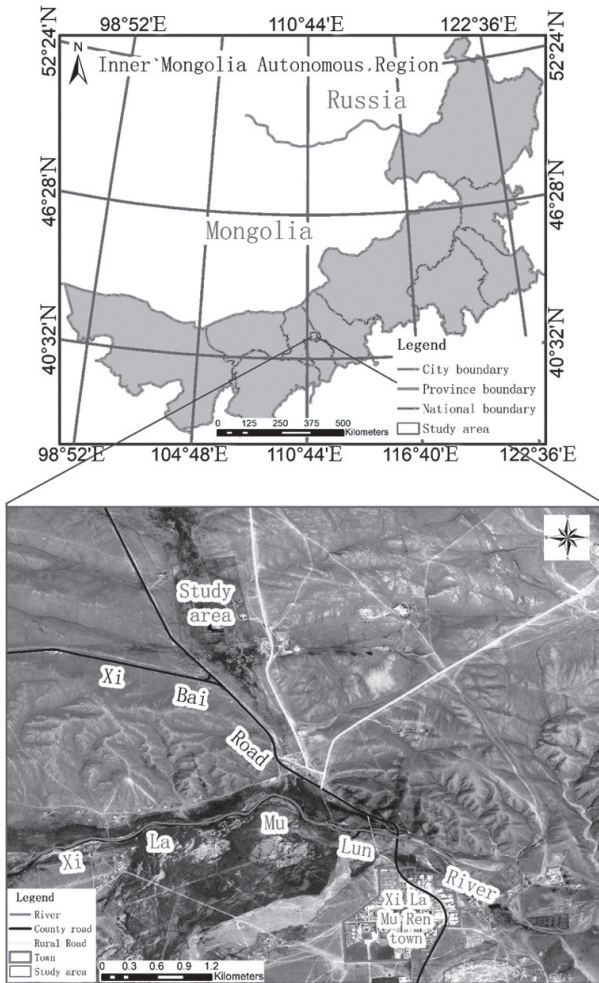


Fig. 1. Location of study area.

Institute of Water Resources for Pastoral Areas of China. Slope, topography, soil texture and vegetation cover were the same for the two stations. Data include soil moisture, soil heat flux, precipitation, solar radiation and four-component radiation data (downward shortwave, upward shortwave, downward longwave, upward longwave). Of these, the ENVIS station collected soil heat flux, solar radiation and four-component radiation data. The UGT system collected soil moisture and precipitation data. Table 1 lists sensor information and settings. The time resolution of precipitation data was

5 min. Precipitation data were converted into daily precipitation as accumulation. Other data were binned in 10 min intervals. Daily average value for each day was calculated as a cumulative average.

According to the four-component radiation data, the net shortwave radiation (R_s), net longwave radiation (R_l), surface albedo (α) and net surface radiation (R_n) were calculated by the following respective formulas:

$$R_s = R_{sd} - R_{su} \tag{1}$$

$$R_l = R_{ld} - R_{lu} \tag{2}$$

$$\alpha = \frac{R_{su}}{R_{sd}} \times 100\% \tag{3}$$

$$R_n = R_l + R_s \tag{4}$$

In these expressions, R_{sd} is surface receiving shortwave radiation, R_{su} is surface reflecting shortwave radiation, R_{ld} is surface receiving longwave radiation, R_{lu} is surface reflecting longwave radiation. These terms are all calculated in units of $W \cdot m^{-2}$. The dimensionless term α represents surface albedo.

Subtracting the soil heat flux from the calculated R_n gives the total flux as follows:

$$H + LE = R_n - Q_a \tag{5}$$

In this expression, H is the sensible heat flux, LE is the latent heat flux, $H + LE$ is the total flux and Q_a is the soil heat flux, all in units of $W \cdot m^{-2}$.

IBM SPSS® Statistics 25 software was used to conduct outlier tests on the data and eliminate abnormal data. Standard correlation analysis tools in Microsoft Excel were used to calculate correlation statistics. Images were drafted in Origin 2018 software.

Data Screening and Division of Dry and Wet Intervals

Atmospheric convection activity in the study area was stronger in summer. The June to August data from 2010 to 2018 were therefore selected for detailed analysis. The analysis focused on data collected from 06:00 to 18:00 Beijing time. Atmospheric conditions

Table 1. Details of each sensor.

Model	Name	Quantity	Note
HFP-01	Soil heat flux sensor	3	Measurement range of $\pm 2000 W \cdot m^{-2}$, $1 W \cdot m^{-2}$ accuracy, installed at 5 cm depth.
CNR1	Net radiation sensor	1	$1 W \cdot m^{-2}$ accuracy, installed at 1.5 m height.
161050 UGT	Rain gauge	1	Non-heated, 0.1 mm accuracy.
162100 UGT	Solar radiation sensor	1	Measurement range of $0-1400 W \cdot m^{-2}$, $1 W \cdot m^{-2}$ accuracy.
Trime-IT TDR	Soil moisture sensor	1	Accuracy: $\pm 1\%$ at 0-40% water content, $\pm 2\%$ at 40-70% water content, precision of $\pm 0.5\%$, installed at 5 cm depth.

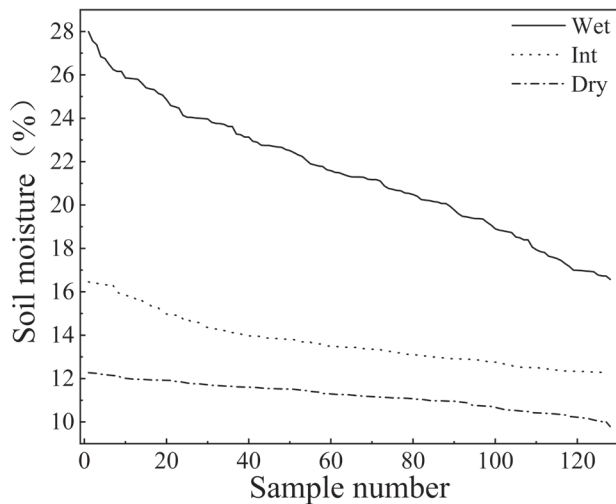


Fig. 2. Sample distribution for dry, intermediate and wet intervals.

strongly influence the surface response to solar radiation and atmospheric reverse radiation [26, 27]. This study only analyzed data collected during fair weather in order to reduce the interference of atmospheric conditions on the flux transfer between ground and air. These processing steps eliminated days with daily rainfall greater than 0. Data with R_{sd} greater than $400 \text{ W}\cdot\text{m}^{-2}$ were interpreted to represent fair weather. This gave a total of 383 days of analyzable data. Fig. 2 shows data arranged in ascending order according to soil moisture, which itself is divided into wet, intermediate and dry intervals. These intervals represent 128, 127 and 128 days, respectively. Table 2 list interval characteristics.

Results and Discussion

Diurnal Variation in Radiation and Water-Heat Flux under Different Soil Moisture Conditions

Fig. 3a) shows the daily change in albedo under different soil moisture conditions. In general, albedo increases from 6:00 to 8:00 and then declines after 8:00. Albedo stabilizes by 9:30 and then persists at the same value until 18:00. The three intervals showed significant differences among themselves ($P < 0.01$) during this stable period. Similar to results from other studies, morning and afternoon hours also showed significant differences in albedo [28-31]. Surface albedo varies

considerably before and after sunrise (6:00-9:00). This relates to condensation of dew on vegetation. The dew scattering effect can cause aberrant increases in surface albedo during morning hours in arid environments [32]. During afternoon hours, surface conditions are relatively stable. These translate to relatively stable surface albedo trends.

As shown in Fig. 3b), daily variation in net surface radiation (R_n) is unimodal. Maximum R_n values during dry, intermediate and wet intervals were $565.11 \text{ W}\cdot\text{m}^{-2}$, $576.92 \text{ W}\cdot\text{m}^{-2}$ and $647.66 \text{ W}\cdot\text{m}^{-2}$, respectively. The R_n data showed similar trends under different soil moisture conditions but R_n did not show significant differences between dry and wet intervals ($P < 0.01$), especially between 10:00 and 14:00.

The soil heat transfer term Q_a represents energy exchange between the soil and the atmosphere with positive and negative values indicating direction. Positive Q_a values indicate that the atmosphere transfers heat to the soil. Negative Q_a values indicate that the soil transfers heat to the atmosphere. Fig. 3c) shows clear, unimodal daily variation in Q_a . From 6:00 to 8:00 a.m., Q_a is negative indicating heat transfer to the atmosphere. After 8:00 a.m., positive Q_a values indicate heat transferred to the soil. The difference in Q_a between dry, intermediate and wet intervals became largest between 10:00 and 14:00, when data reached the $P < 0.05$ significance level. The maximum difference in Q_a between dry and wet intervals was $15.51 \text{ W}\cdot\text{m}^{-2}$ indicating that soil moisture exerts a strong influence on Q_a .

Total flux data in this study was calculated according to formula (5). Fig. 3d) shows the daily change in total flux, which was broadly consistent with the daily change in R_n . Each soil moisture interval showed increasing trends from 6:00 to 12:00 and decreasing trends from 12:00 to 18:00. The total flux for dry and intermediate intervals reached maximum respective values of $494.67 \text{ W}\cdot\text{m}^{-2}$ and $500.90 \text{ W}\cdot\text{m}^{-2}$ at 12:00. The maximum total flux of $559.55 \text{ W}\cdot\text{m}^{-2}$ for the wet interval occurred at 11:30. Minimum values for wet, intermediate and dry intervals ($7.38 \text{ W}\cdot\text{m}^{-2}$, $-0.65 \text{ W}\cdot\text{m}^{-2}$ and $9.45 \text{ W}\cdot\text{m}^{-2}$, respectively) occurred at 6:00. Total flux values from 6:00 to 10:00 did not vary for dry and wet intervals. Total flux values from 10:00 to 14:00 however did show significant differences between dry and wet intervals ($P < 0.01$).

As shown in Fig. 4a), daily variation in net shortwave radiation (R_s) is consistent with variation trends in net

Table 2. Descriptive statistics for soil moisture and solar radiation for dry, intermediate and wet intervals.

	Sample size (days)	Soil moisture (%)						Solar radiation ($\text{W}\cdot\text{m}^{-2}$)		
		Mean	Max	Min	Range	SD	CV	Mean	SD	CV
Wet	128	21.52	28.00	16.57	11.43	2.89	0.13	564.8	71.9	0.13
Int	127	13.70	16.46	12.27	4.19	1.14	0.08	550.2	72.1	0.13
Dry	128	11.21	12.27	9.78	2.49	0.61	0.05	563.6	71.5	0.13

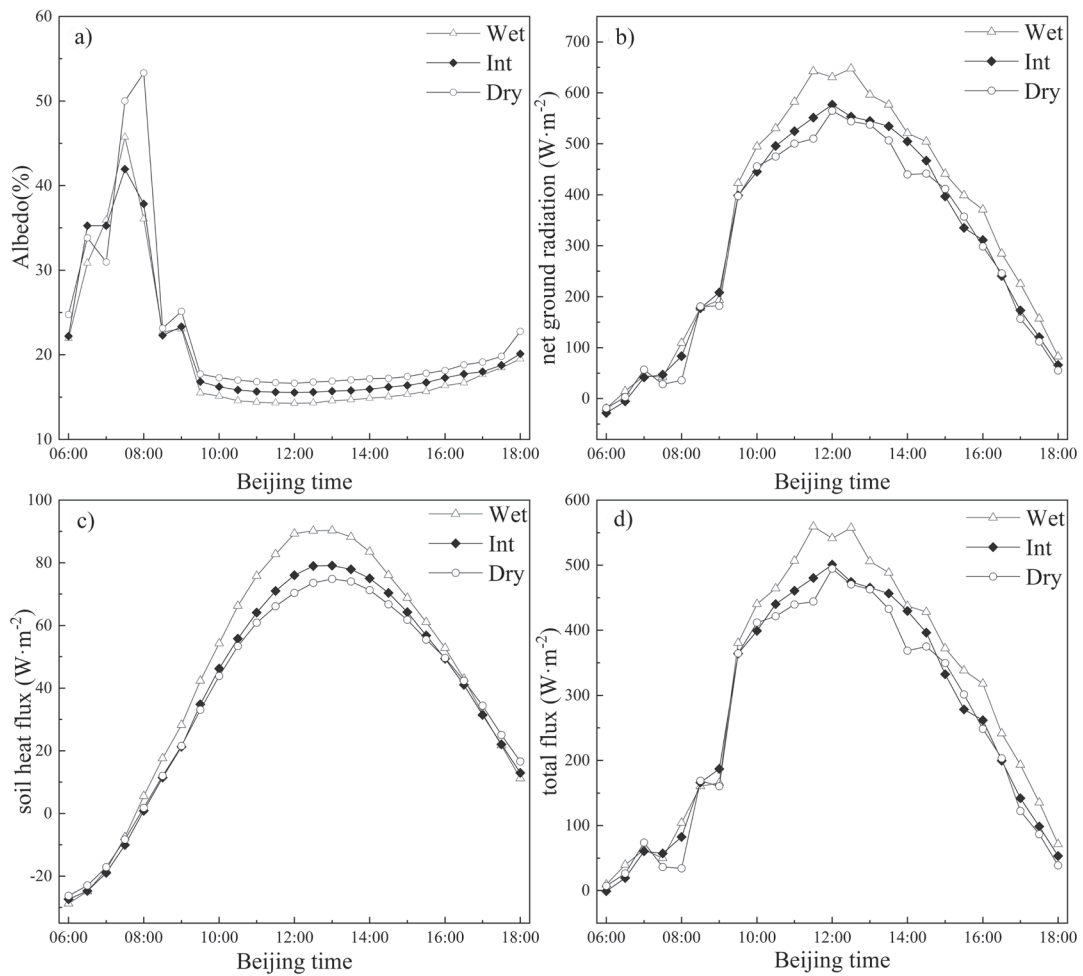


Fig. 3. Diurnal variation in albedo a), net ground radiation b), soil heat flux c) and total flux d) for dry, intermediate and wet intervals.

surface radiation (R_p). In the morning (6:00 to 12:00), R_s increased, reached a maximum by noon, and then began to decline until 18:00. Maximum values for dry, intermediate and wet intervals were $759 W \cdot m^{-2}$, $748.11 W \cdot m^{-2}$ and $794.6 W \cdot m^{-2}$, respectively. Different soil moisture intervals showed no obvious differences

in R_s . By contrast, net longwave radiation (R_l) was significantly different for different soil moisture conditions ($P < 0.01$). As shown in Fig. 4b), the maximum value for R_l occurs at 6:00. Dry, intermediate and wet interval R_l values were $-61.73 W \cdot m^{-2}$, $-58.05 W \cdot m^{-2}$ and $-50.33 W \cdot m^{-2}$, respectively. As time progressed,

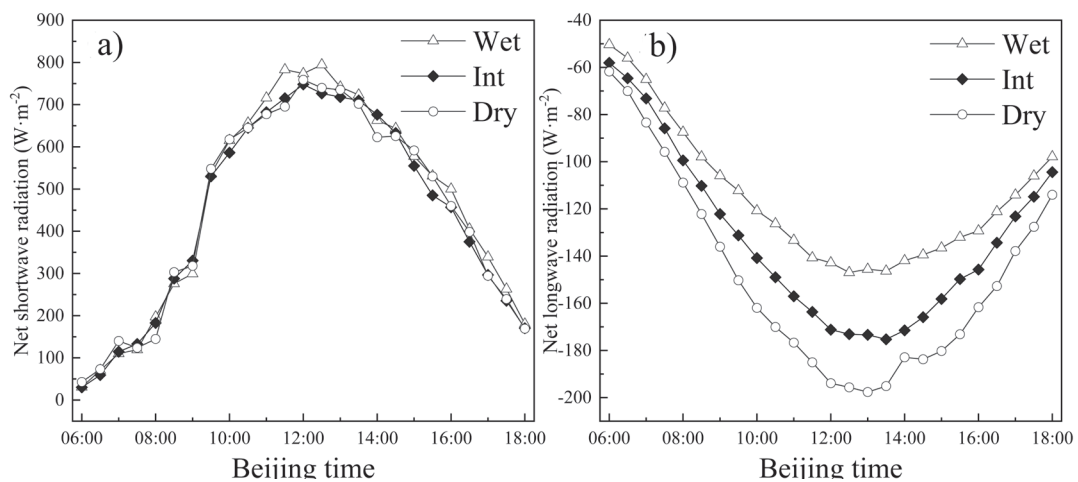


Fig. 4. Diurnal variation in a) net shortwave radiation and net b) longwave radiation under different moisture conditions.

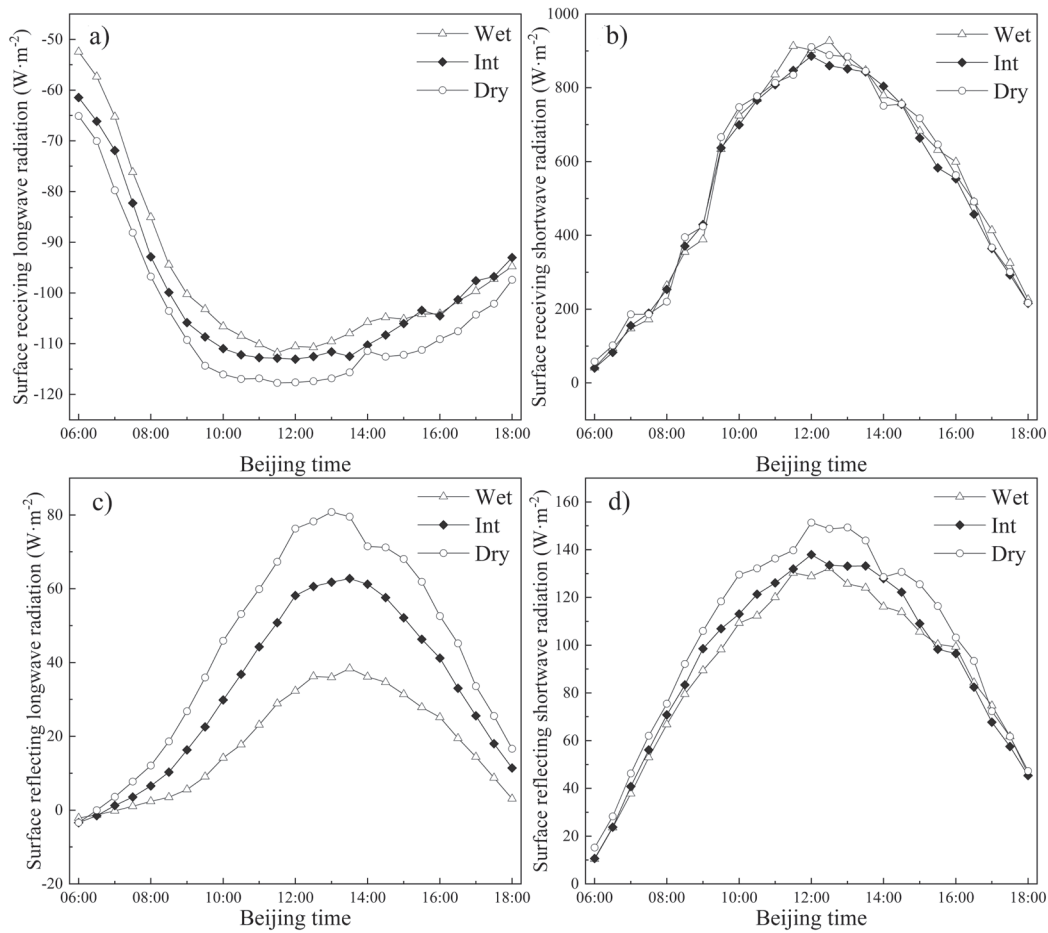


Fig. 5. Daily changes in R_{sd} a), R_{su} b), R_{ld} c), and R_{lu} d) for dry, intermediate and wet intervals.

R_l decreased as did differences from different soil moisture conditions. R_l values showed their greatest divergence among dry, intermediate and wet intervals at 13:00. These were $-197.63 \text{ W}\cdot\text{m}^{-2}$, $-173.39 \text{ W}\cdot\text{m}^{-2}$ and $-145.57 \text{ W}\cdot\text{m}^{-2}$. After 13:00, R_l began to rise while the differences in R_l for different moisture intervals gradually decreased. The R_l parameter showed a more obvious response to soil moisture compared to R_s . Soil moisture apparently influences daily changes in R_n through daily changes in R_l .

Daily changes in R_{sd} , R_{su} , R_{ld} and R_{lu} for dry, intermediate and wet intervals were analyzed to evaluate soil moisture as a mechanism in generating differences in daily variation of surface radiation and water-heat flux. As shown in Fig. 5a), R_{ld} first declines and then increases. The other three radiation fluxes show a single-peak trend that first increases and then decreases.

Soil moisture exerts the strongest influence on daily changes in R_{lu} ($P \leq 0.01$) followed by R_{su} . Soil moisture

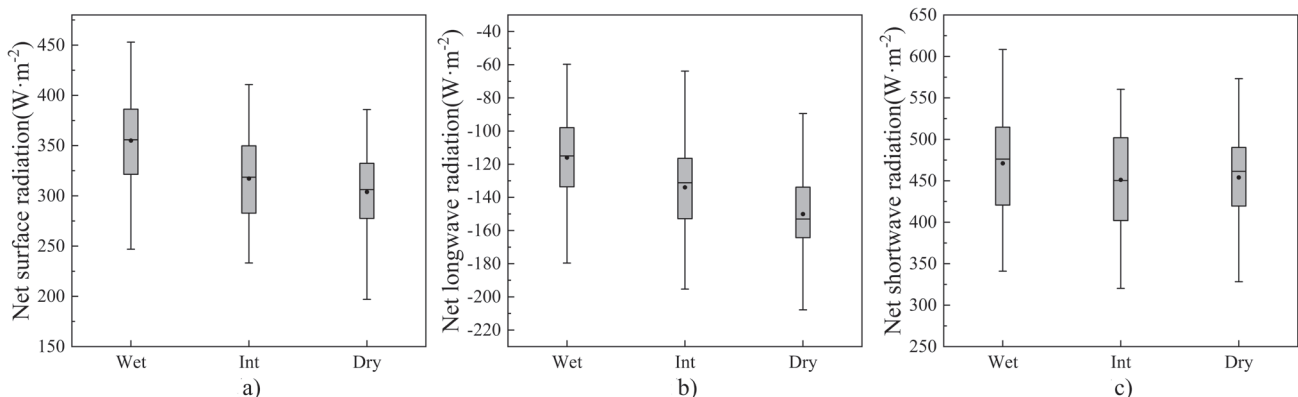


Fig. 6. Data ranges for net surface radiation a), net longwave radiation b) and net shortwave radiation c).

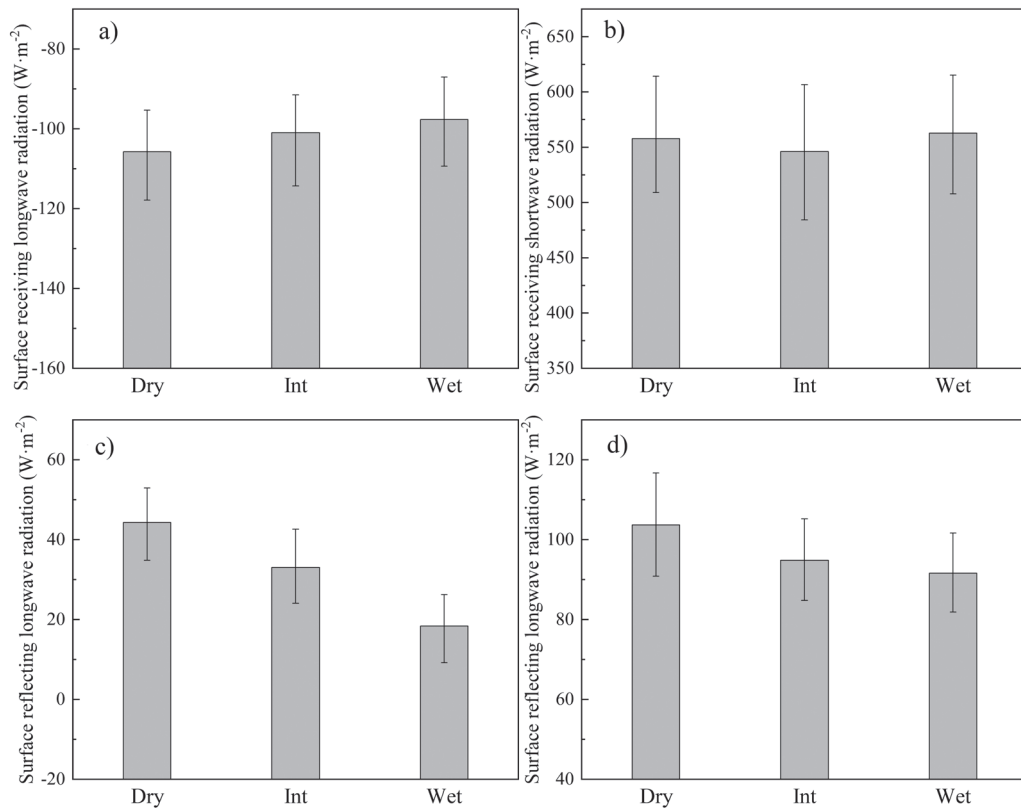


Fig. 7. Histograms for R_{sd} a), R_{su} b), R_{ld} c), and R_{lu} d) for dry, intermediate and wet intervals.

does not apparently influence longwave and shortwave radiation received by the surface. Radiant flux depends mainly on the surface's reflection capacity, rather than on absorption capacity. Soil moisture thus shows a stronger relationship with longwave radiation than with shortwave radiation. This also explains the greater sensitivity of R_l to changes in soil moisture relative to R_s . Soil moisture variation itself depends on land surface. In desert steppe environments, precipitation can supplement soil humidity especially during summer months experiencing concentrated precipitation events. Precipitation throughout the year has thus become an important indicator of dry and wet conditions in arid and semi-arid climate regions. Zhang Qiang et al. [33] used CLM model simulation data to show that drier climate conditions will cause an increase in R_{lu} and a decrease in surface absorbing longwave radiation. Similar to the findings of this research, these factors reduce Q_a and R_n flux.

Radiant flux data indicate that daily changes in R_n , Q_a , total flux, R_s and four radiation components (except R_{ld}) all appear as a unimodal peak. The increase and subsequent decrease in values are consistent with results of previous studies [34-39]. The observed distributions may relate to diurnal variation in solar radiation, which serves as the main source of energy for the Earth's surface [40-41]. However, the solar altitude angle and atmospheric conditions can also influence insolation. Solar altitude angle is a primary factor in insolation for cases excluding cloudy and rainy days. Change in solar

altitude angle directly influences radiant flux received at the surface. This indirectly influences daily changes of other hydrothermal and radiant fluxes [42]. Periods with the most significant differences in hydrothermal and radiant fluxes under different soil moisture conditions all occurred between 10:00-14:00. During this time, a high solar altitude angle and strong solar radiation induced a period of strong ground-air coupling around noon. This also enhanced the sensitivity of radiation and water-heat flux to soil moisture. Further research can help confirm and identify causes for this phenomenon.

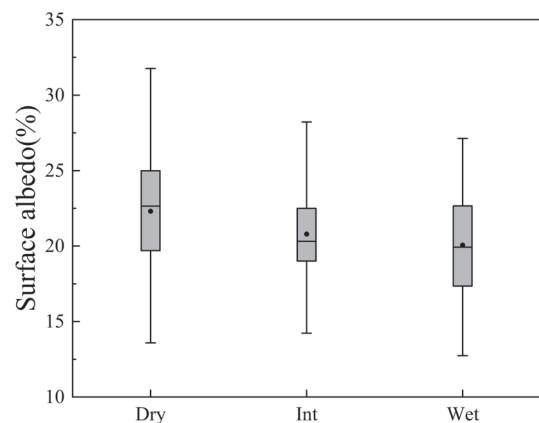


Fig. 8. Surface albedo ranges.

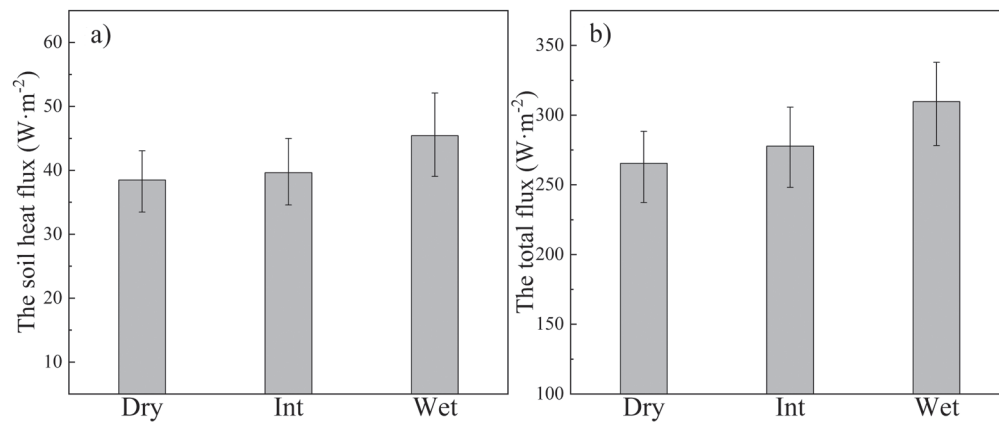


Fig. 9. Distribution of soil heat fluxes a) and the total flux b) under dry, intermediate and wet intervals

Distribution of Radiation Flux under Different Moisture Conditions

To further evaluate the effects of soil moisture on different types of radiation flux, we analyzed data distributions. Both net radiation and R_l show a significant decrease with decreasing soil moisture. Dry, intermediate and wet intervals show obvious differences between the upper quartile, median, average and lower quartile values. Intervals show large differences in their mean values for net radiation (e.g. 51.12 W·m⁻²; solid points within bars shown in Fig. 6). Net radiation showed more subtle variation relative to soil moisture. The R_s data did not vary significantly with soil moisture. This indicates that soil moisture affects longwave and shortwave radiation between the surface and atmosphere. Fig. 7a) shows R_{ld} distributions for wet, intermediate and dry intervals. As soil moisture increases, R_{ld} decreases.

Fig. 7c) and d) show histograms for longwave and shortwave radiation (respectively) reflected from the

ground under different moisture conditions. Both longwave and shortwave radiation reflected from the ground surface decrease with greater soil moisture. Surface reflection capacity is also affected by soil moisture. Relative to shortwave radiation reflected from the ground surface, R_{lu} shows much more variation in response to soil moisture. By contrast, R_{sd} does not vary according soil moisture conditions (Fig. 7b). In summary, changes in soil moisture apparently affect the ground surface's reflective capabilities. Effect on R_{lu} are strongly evident. Soil moisture exerts a stronger influence on longwave radiation than on shortwave radiation.

Fig. 8 shows the distribution of surface albedo which does not differ significantly for dry, intermediate and wet intervals. Soil moisture therefore does not strongly influence surface albedo. Dry, intermediate and wet intervals gave albedo values of 22.5%, 20.8% and 20%, respectively. The maximum, upper quartile, median, lower quartile and minimum values for the dry and wet intervals show only small differences in surface

Table 3. Correlation between soil moisture, radiation and water-heat flux.

	Totality	Dry	Int	Wet
Surface receiving longwave radiation (R_{ld})	0.212**	0.035	-0.009	0.243**
Surface receiving shortwave radiation (R_{sd})	0.076	0.01	0.02	0.12
Surface reflecting longwave radiation (R_{lu})	-0.678**	-0.143	-0.197*	-0.582**
Surface reflecting shortwave radiation (R_{sl})	-0.296**	-0.151	-0.038	-0.244**
Net shortwave radiation (R_s)	0.173**	0.062	0.035	0.194*
Net longwave radiation (R_l)	0.511**	0.094	0.089	0.459**
Net surface radiation (R_n)	0.513**	0.146	0.103	0.476**
Surface albedo	-0.279**	-0.196*	0.14	-0.305**
Soil heat flux (Q_a)	0.345**	0.231**	0.056	0.101
The total flux	0.5**	0.115	0.099	0.503**

Note: * indicates significant correlation at P<0.05 significance level; ** indicates significant correlation at the P<0.01 significance level; (Sample size: n = 383 of which dry interval n = 128, intermediate interval n = 127 and wet interval n = 128).

albedo. Change in soil moisture thus do not cause major changes in surface albedo for the study area.

Total flux represents the sum of sensible heat transfer (turbulence, convection) and latent heat transfer (evaporation, transpiration). Q_a and total flux serve as the main processes in heat transfer between the ground and the atmosphere. Fig. 9 shows that with increasing soil moisture, both Q_a and total flux increase. Relative to Q_a , total flux shows greater variation with soil moisture. The mean value of total flux under dry and wet conditions differed by $44.23 \text{ W}\cdot\text{m}^{-2}$, while the mean value for Q_a differed by only $6.94 \text{ W}\cdot\text{m}^{-2}$ under different dry and wet conditions.

Correlation Analysis of Radiation, Water-Heat Flux and Soil Moisture

The R_{ld} , R_{su} , R_{lu} , R_p , R_s , R_n , albedo, Q_a and total flux parameters all show differing degrees of covariation with soil moisture. To further evaluate the influence of soil moisture on various radiant fluxes and water-heat fluxes, we performed correlation analysis of these variables and different soil moisture intervals.

Correlation analysis detected significant positive correlation between soil moisture and R_{ld} , R_s , R_p , R_n , Q_a and total flux ($P < 0.01$). Soil moisture was strongly negatively correlated with R_{lu} and R_{su} ($P < 0.01$). Soil moisture showed no correlation with R_{sd} . For the dry interval, soil moisture (9.78-12.27%) exhibited a significant negative correlation with surface albedo ($P < 0.05$), significant positive correlation with Q_a ($P < 0.01$) but showed no correlations with other variables. Soil moisture for the intermediate interval (12.27-16.46%) was only significantly negatively correlated with R_{lu} ($P < 0.05$) but showed no correlation with other variables. The wet interval (16.57-28%) exhibited a very significant positive correlation with the surface receiving longwave radiation, R_p , albedo and total flux ($P < 0.01$). The wet interval also showed a significant positive correlation with R_s ($P < 0.05$) and a very significant negative correlation with R_{lu} , R_{su} and surface albedo ($P < 0.01$). This indicates that as the soil moisture rises, the correlation between longwave radiation received by the ground and soil moisture significantly increases. (Table 3).

Correlation analysis found that soil moisture correlated negatively with surface albedo. Zhang Guo et al. reported a similar relationship [43]. Zhang Lele et al. [44] and Ma Yingsai et al. [45] also found that the albedo measured from the Qinghai-Tibet Plateau and the Loess Plateau decreased significantly with increasing soil moisture. This indicates that Q_a correlates positively with soil moisture. Chen Hai-cun et al. [46] report similar findings. The present research also showed that Q_a exhibits the greatest variation with soil moisture under dry soil conditions. Total flux showed significant positive correlation with soil moisture under wet conditions. This correlation may arise from the intensification of surface evaporation and

transpiration. Together these could cause turbulence and disruption of atmospheric convection at the ground surface.

Total flux strongly covaried with soil moisture. Increasing soil moisture causes total flux to rise. Numerous studies [47-51] have shown that hydrothermal properties of the underlying surface determine the energy distribution observed at the surface. When underlying soil moisture is high, the energy in the land-air system consists primarily of latent heat. Dry soil conditions result in the system energy taking the form mostly of sensible heat. Soil moisture can strongly influence both sensible and latent heat. Future research should collect sensible and latent heat flux data to future constrain total flux under different soil moisture conditions.

Conclusions

In the desert steppe environment analyzed by this study, surface albedo, R_n , Q_a , total flux, R_s , R_p , R_{ld} , R_{sd} , R_{lu} and R_{su} all showed obvious daily change. Soil moisture affects the diurnal variation ranges for both radiation and water-heat flux. The R_l and Q_a parameters showed the largest variation in response to soil moisture. R_n and the intervals most strongly influenced by soil moisture occurred primarily around noon and in the afternoon. Of the four radiation components, soil moisture exerted the strongest influence on the diurnal variation in R_{lu} , followed by R_{ld} and R_{su} .

Increased soil moisture leads to an increase in net radiation, R_p , R_{ld} , Q_a and total flux but a significant decrease in the surface reflecting longwave and shortwave radiation. Soil moisture did not exert a strong influence on R_{sd} , R_s and surface albedo. Correlation analysis verified that soil moisture correlated negatively with R_{lu} and positively with R_p , R_n and total flux. The higher the soil moisture, the stronger the correlation with R_{lu} . Soil moisture influences the atmospheric system primarily through its influence on total flux (sensible heat and latent heat) and R_n . Future research should measure latent and sensible heat flux to confirm the effects of soil moisture on total flux.

Acknowledgements

This study was supported by the Special fund project of China Institute of Water Resources and Hydropower Research (IWHR) (MK2017J05) and Inner Mongolia Science and Technology Plan Project (201701024).

Conflict of Interest

The authors declare no conflict of interest.

References

1. MA Y., WANG Y., WU R., HU Z., YANG K., LI M., MA W., ZHONG L., SUN F., CHEN X., ZHU Z., WANG S., ISHIKAWA H. Recent advances on the study of atmosphere-land interaction observations on the Tibetan Plateau. *Hydrology and Earth System Sciences*. **13**(7), 1103, **2009**.
2. HUANG J., CHEN W., WEN Z., ZHANG G., LI Z., ZUO Z., ZHAO Q. Review of Chinese atmospheric science research over the past 70 years: Climate and climate change. *Science China Earth Science*. **62**, 1514, **2019**.
3. LI J., LI Y.Q., JIANG X.W., GAO D. Characteristics of land-atmosphere energy exchanges over complex terrain area of Southeastern Tibetan Plateau under different synoptic conditions. *Chinese Journal of Atmospheric Sciences*, **40** (4), 777, **2016**.
4. SENEVIRATNE S.I., CORTI T., DAVIN E.L., HIRSCHI M., JAEGER E.B., LRENE I., ORLOWSKY B., TEULING A.J. Investigating soil moisture-climate interactions in a changing climate: A review. *Earth Science Reviews*. **99** (3-4), 125, **2010**.
5. MARTELLO M., FERRO N.D., BORTOLINI L., MORARI F. Effect of Incident Rainfall Redistribution by Maize Canopy on Soil Moisture at the Crop Row Scale. *Water*. **7** (5), 2254, **2015**.
6. GUO W.D., MA Z.G., YAO Y.H. Regional Characteristics of Soil Moisture Evolution in Northern China over Recent 50 Years. *Acta Geographica Sinica*. (S1), 83, **2003**.
7. DIRMEYER P.A., SHUKLA J. Observational and Modeling Studies of the Influence of Soil Moisture Anomalies on Atmospheric Circulation (Review). *Prediction of Interannual Climate Variations*. Springer Berlin Heidelberg, **1993**.
8. SONG Y.H., HUA L.P. Impact of soil moisture anomalies on seasonal, summertime circulation over North America in a Regional Climate Model. *Journal of Geophysical Research: Atmospheres*. **105**, **2000**.
9. KOSTER R.D., SUAREZ M.J., HIGGINS R.W., VAN DEN DOOL H.M. Observational evidence that soil moisture variations affect precipitation. *Geophysical Research Letters*. **30** (5), 45, **2003**.
10. CHAHINE M. The hydrological cycle and its influence on climate. *Nature*. **359**, 373, **1992**.
11. JAEGER E.B., SENEVIRATNE S.I. Impact of soil moisture-atmosphere coupling on European climate extremes and trends in a regional climate model. *Climate Dynamics*. **36** (9-10), 1919, **2011**.
12. FAN K.K., ZHANG Q., SUN P., SONG C.Q., YU H.Q., ZHU X.D., SHEN Z.X. Effect of soil moisture variation on land surface air temperature over the Tibetan Plateau. *Acta Geographica Sinica*. **75** (01), 82, **2020**.
13. GALLEGO E.B., Taylor C.M., HARRIS P.P., GHENT D. Global observational diagnosis of soil moisture control on the land surface energy balance. *Geophysical Research Letters*. **43** (6), 2623, **2016**.
14. DOUVILLE H. Assessing the Influence of Soil Moisture on Seasonal Climate Variability with AGCMs. *Journal of Hydrometeorology*. **4** (6), 1044, **2003**.
15. ZHANG W.J., ZHOU T.J. A numerical experiment on the effect of soil moisture to summer climate over China. *Acta Meteorologica Sinica*. **2012**.
16. ZHANG R.H., LIU L., ZUO Z.Y. Variations of soil moisture over China and their influences on Chinese climate. *Chinese Journal of Nature*. **38** (05), 313, **2016**.
17. ZUO Z.Y., ZHANG R.H. Influence of Soil Moisture in Eastern China on the East Asian Summer Monsoon. *Advances in Atmospheric Sciences*. **2**, 151, **2016**.
18. SANTANELLO J.A., PETERS-LIDARD C.D., KUMAR S.V. A modeling and observational framework for diagnosing local land-atmosphere coupling on diurnal time scales. *Journal of Hydrometeorology*. **10** (3), 577, **2009**.
19. KOSTER R.D., GUO Z.C., DIRMEYER P.A., BONAN G. GLACE: The Global Land-Atmosphere Coupling Experiment. Part I: overview. *Journal of Hydrometeorology*. **7** (4), **2006**.
20. ZHANG J., WANG W.C., WEI J. Assessing land-atmosphere coupling using soil moisture from the Global Land Data Assimilation System and observational precipitation. *Journal of Geophysical Research*. **113** (D17), D17119, **2008**.
21. WANG S.Y., ZHANG Y., LU S.H., SHANG L.Y., ZHANG S.B. Seasonal Variation Characteristics of Radiation and Energy Budgets in Alpine Meadow Ecosystem in Maqu Grassland. *Plateau Meteorology*. **31** (03), 605, **2012**.
22. GE J., YU Y., LI Z.C., XIE J., LIU C., ZAN B.L. Impacts of freeze/thaw processes on land surface energy fluxes in the permafrost region of Qinghai-Xizang Plateau. *Plateau Meteorology*. **35** (3), 608, **2016**.
23. SU Y.R., LV S.H., FAN G.Z. The characteristics analysis on the summer atmospheric boundary layer height and surface heat fluxes over the Qinghai-Tibetan Plateau. *Plateau Meteorology*. **37** (6), 1470, **2018**.
24. CHEN H.S., ZHOU J. Impact of Interannual Soil Moisture Anomaly on Simulation of Extreme Climate Events in China. Part II: Sensitivity Experiment Analysis. *Chinese Journal of Atmospheric Sciences*. **37** (01), 1, **2013**.
25. ZHANG G., KANG Y., HAN G., SAKURAI K. Effect of climate change over the past half century on the distribution, extent and NPP of ecosystems of Inner Mongolia. *Global Change Biology*. **17** (1), 377, **2011**.
26. YAMADA K., HAYASAKA T., Iwabuchi H. Contributing Factors to Downward Longwave Radiation at the Earth's Surface. *Scientific online letters on the atmosphere: SOLA*. **8**, 94, **2012**.
27. DIAZ-TORRES J.J., HERNANDEZ-MENA L., MURILLO-TOVAR M.A., LEON-BECERRIL E. Assessment of the modulation effect of rainfall on solar radiation availability at the Earth's surface. *Meteorological Applications*. **24** (2), **2017**.
28. XU A.L., LI J., SUN J.H., LIU J.S., ZHAO X.H. Analyses on Micrometeorology Characteristic and Energy Exchange in Surface Layer in Dali Region of the Southeastern Margin of Tibetan Plateau. *Plateau Meteorology*. **32** (01), 9, **2013**.
29. YAO T., ZHANG Q. Study on land-surface albedo over different types of underlying surfaces in North China. *Acta Physica Sinica*. **63** (08), 460, **2014**.
30. LI D.S., WANG J.Y., WANG S.G., LI Z.C., SHANG K.Z., SHI J.S. Change Features of Surface Albedo of Semi-Arid Grassland over the Loess Plateau of Middle Part Gansu. *Plateau Meteorology*. **33** (01), 89, **2014**.
31. YANG J.X., LI Z.C., WEI Z.G., GAO X.Q., ZHENG Z.Y., HOU X.H. Characteristics of solar spectral radiation and corresponding albedo in sparse vegetation region. *Acta Energetica Solaris Sinica*. **38** (03), 852, **2017**.
32. BAI X.X., HUANG X.L., QIN M.S., ZHANG Y.F., CHEN L.G., GUO Z., HAO L. Characteristics of surface albedo in subtropical paddy rice fields. *Chinese Journal of Eco-Agriculture*. **25** (11), 1707, **2017**.

33. ZHANG Q., HUANG J., ZHANG L., ZHANG L.Y. Warming and drying climate over Loess plateau area in China and its effect on land surface energy exchange. *Acta Physica Sinica*. **62** (13), 561, **2013**.
34. ZHAO X.B., PENG B., QIN N.S., WANG W. Characteristics of Energy Transfer and Micrometeorology in Surface Layer in Different Areas of Tibetan Plateau in Summer. *Plateau and Mountain Meteorology Research*. **31** (01), 6, **2011**.
35. XU Z.W., LIU S.M., XU T.R., DING C. The Observation and Calculation Method of Soil Heat Flux and Its Impact on the Energy Balance Closure. *Advances in Earth Science*. **28** (08), 875, **2013**.
36. QI Y., FANG S.B., ZHOU W.Z. Correlative analysis between the changes of surface solar radiation and its relationship with air pollution, as well as meteorological factor in East and West China in recent 50 years. *Acta Physica Sinica*. **64** (08), 398, **2015**.
37. HUANG T.Y., LIU T.X., DUAN L.M., LI D.F., WANG G.L., CHEN X.Q. Characteristics of Water and Heat Fluxes and Its Footprint Climatology in Horqin Cascade Ecological Zone. *Journal of Desert Research*. **39** (06), 30, **2019**.
38. XIE Y., WEN J., LIU R., WANG X., JIA D.Y. An initial analysis of characteristics of radiation budget near ground in alpine wetland in source area of the yellow river. *Acta Energetica Solaris Sinica*. **40** (01), 1, **2019**.
39. ZHANG F.W., HAN Y., LI H.Q., LI Y.N., CAO G.M., ZHOU H.K. Turbulent Heat Exchange and Partitioning and Its Environmental Controls between the Atmosphere and an Alpine Potentilla Fruticosa Shrublands over the Qinghai-Tibetan Plateau. *Chinese Journal of Agrometeorology*. **41** (02), 76, **2020**.
40. ZHANG L., WANG C., FU S.Y. Solar Variation and Global Climate Change. *Chin. J. Space Sci.* **31** (05), 549, **2011**.
41. ZHANG X.T., LIANG S.L., WANG G.X., YAO Y.J. Evaluation of the Reanalysis Surface Incident Shortwave Radiation Products from NCEP, ECMWF, GSFC, and JMA Using Satellite and Surface Observations. *Remote Sensing*. **8** (3), 225, **2016**.
42. ZHOU Y., GAO X.Q., LI Z.C., HUI X.Y., YANG L.W. Analysis of the characteristics of deep soil heat flux in Qinghai-Tibetan Plateau. *Plateau Meteorology*. **36** (2), 307, **2017**.
43. ZHANG G., ZHOU G.S., YANG F.L. Analysis on dynamic characteristics of surface albedo over a desert steppe in Inner Mongolia. *Acta Ecologica Sinica*. **30** (24), 6943, **2010**.
44. ZHANG L.L., ZHAO L., LI R., GAO L.M., XIAO Y., QIAO Y.P., SHI J.Z. Investigating the influence of soil moisture on albedo and soil thermodynamic parameters during the warm season in Tanggula Range, Tibetan Plateau. *Journal of Glaciology and Geocryology*. **38** (02), 351, **2016**.
45. MA Y.S., MENG X.H., HAN B., YU Y., LV S.H., LUAN L., LI G.W. Observations of Soil Moisture Influence on Surface Energy Dynamics and Planetary Boundary Layer Characteristics over the Loess Plateau. *Plateau Meteorology*. **38** (04), 705, **2019**.
46. CHEN H.C., LI X.D., LI F.X., ZHOU B.R., LI C.Y. Change of Soil Temperature and Soil Moisture Content in Typical Degenerated Steppe in Maduo County in the Headstream Region of the Yellow River. *Arid Zone Research*. **30** (01), 35, **2013**.
47. ZHOU D.G., HUANG G., MA Y.M., Summer heat transfer over a Gobi underlying surface in the arid region of Northwest China. *Trans Atmos Sci*. **35** (5), 541, **2012**.
48. ZENG J., ZHANG Q. A comparative study of the characteristics of the clear-sky land surface processes over the different underlying surfaces in the northern part of China during July-September 2008. *Acta Meteorologica Sinica*. **70** (04), 821, **2012**.
49. YUE P., ZHANG Q., WANG S., WANG R.Y., LI H.Y., WANG R.A. Characteristics of Soil Temperature, Moisture and Heat Pro- and Post-precipitation in Semiarid Grassland over Longzhong Loess Plateau. *Journal of Desert Research*. **33** (06), 1766, **2013**.
50. LIU B., ZHAO W.Z., WEN Z.J., ZHANG Z.H. Response of water and energy exchange to the environmental variable in a desert-oasis wetland of Northwest China. *Hydrological Processes*. **28** (25), 6098, **2014**.
51. ZHANG H., FAN G.Z., ZHANG Y.L., LAI X. Numerical Simulation of the Effect of Soil Moisture on a Case of Plateau Vortex over Qinghai-Tibetan Plateau. *Plateau Meteorology*. **37** (04), 886, **2018**.